Contribution from the Inorganic Chemistry Laboratory,
University of Oxford, Oxford OX1 3QR, U.K.

Applications of Two-Photon Spectroscopy to Inorganic Compounds. 1. Spectrum and Electronic Structure of $Cs_2UO_2Cl_4$

Trevor J. Barker, Robert G. Denning,* and Jonathan R. G. Thorne

Received November 3, 1986

The single-crystal polarized two-photon absorption spectrum of $Cs_2UO_2Cl_4$ at 4.2 K is reported. The spectrum is much more highly resolved than the single-photon spectrum and clearly reveals the electronic origin transitions for 13 of the 14 excited states present in the region below 33 000 cm^{-1}. The frequencies of a number of gerade excited-state vibrational modes are readily determined and indicate a very small change in the charge distribution within the UO_2^{2+} ion accompanying the excitation. The strong coupling of the rocking mode of this ion is also apparent. The two-photon polarization data confirm the symmetries of the states and demonstrate that, in some cases, the vibronic intensity arises from interactions in the virtual state coupled by the radiation field. The sign of the tetragonal field splitting is not consistent with the predictions of recent ab initio calculations.

Introduction

In chromophores with inversion symmetry a two-photon transition, induced by the electric-dipole mechanism, is parity-conserving; it creates excited states that, because they are electric-dipole-forbidden in one-photon absorption (OPA), provide complementary data on the characteristics of the electronic and vibrational states. The two-photon absorption (TPA) technique has been extensively applied to organic chromophores.[1] However, despite the intrinsic parity conservation in f–f and d–d electronic transitions, there are only a few examples of applications to f- and d-block elements; these include some recent work on lanthanide compounds,[2] almost exclusively with the f^7 configuration, and d–s transitions in some copper(I) and silver(I) halides.[3] This difference in emphasis is a result of the characteristics of the pulsed laser sources that are essential for the two-photon experiment. Organic chromophores with excited-state energies exceeding 30 000 cm^{-1}, and lanthanide ions with the f^7 configuration, are accessible to the output of the widely used and inexpensive nitrogen laser pumped dye laser; however, realistic output pulse energies are only available for photon energies exceeding 14 000 cm^{-1}. Two commercial laser systems can now provide the longer wavelengths needed to cover the majority of d–d or f–f transitions. Excimer pumped dye lasers can supply photons with energies in the range from 10 000 to 14 000 cm^{-1},[4] although the dye conversion efficiencies and photochemical stabilities are unsatisfactory for routine spectroscopy. Alternatively, stimulated Raman scattering by high-pressure hydrogen provides first and second Stokes waves that are red-shifted from the dye fundamental by 4160.2 and 8320.4 cm^{-1}, respectively. When applied to the output of the dyes that operate between 14 000 and 18 000 cm^{-1}, which can be efficiently pumped by the second harmonic of the Nd-YAG laser, the shifted output gives a convenient source of photons with energies exceeding 6000 cm^{-1}, allowing two-photon access to states with energies in excess of 12 000 cm^{-1}. These sources therefore open up the study of a large number of inorganic chromophores to the two-photon technique. A first report has been made of the spectroscopy of the MnF_6^{4-} ion using such a source.[5] Because two-photon absorption is most readily detected by the excitation of luminescence, only those materials that emit can be studied easily, and care must be taken to protect the luminescence detector from laser radiation.

There are important differences in information content in the OPA and TPA spectra of d–d and f–f transitions. In an octahedral site the OPA spectrum is usually dominated by three electric-dipole-allowed "false" origins, which reflect the coupling of the ungerade local modes of the octahedron, while the magnetic-dipole- or electric-quadrupole-allowed pure electronic origins are often too weak to identify. The ungerade "false" origins have associated vibrational structure in gerade modes that may include those which are Jahn–Teller-active for which the potential can be strongly anharmonic. The spectrum is often broadened by this complexity to a degree that makes its full assignment intractable. Furthermore, the dipolar character of some of the ungerade modes confers on them a relatively large dispersion with wave vector that can be significant at rather long intersite distances. As an illustration, compare the coupling of the symmetric and antisymmetric stretching modes of a one-dimensional array of symmetric triatomic molecules in the simple, but unlikely, case that their axes are parallel to the array axis. Assuming equal charge displacements in the two types of modes, the dispersion in the dipolar asymmetric stretching mode will exceed that due to the quadrupolar coupling of the symmetric modes, providing that the lattice parameter exceeds $6^{1/2}$ of the bond length. With atoms of any real size, this condition is inevitably satisfied in this orientation. The ratio of the dispersion of the two modes increases as the square of the intermolecular distance.

In general the spectral dispersion of the ungerade modes often reflects a structured phonon density of states that adds to the complexity in OPA. By contrast, TPA primarily displays the pure electronic transitions. Although the electronic states may well have a significant dispersion, the constraint that $\mathbf{k} = 0$ gives these origin transitions a homogeneous width determined by coherence and lifetime considerations. In TPA, coupled gerade modes should exhibit small dispersions compared to their ungerade counterparts in OPA.

As an illustration of the power of the technique we report here the TPA spectrum of $Cs_2UO_2Cl_4$. This material is particularly well-suited to the TPA experiment in that its OPA spectrum shows much detail and complexity with a first excited state near 20 000 cm^{-1}. The luminescence has almost unit quantum efficiency and is easily detected by photomultipliers. Further, the characterization of the excited states by OPA has been a difficult and controversial task, the main problem being the correct identification of the excited-state configurations.

The electronic spectrum and structure of the uranyl ion have been the subject of a number of experimental and theoretical studies.[6–11] One current view is that the first excited configu-

* To whom correspondence should be addressed.

(1) (a) Goodman, L.; Rava, R. P. *Acc. Chem. Res.* **1984**, *17*, 250. (b) Birge, R. R. *Acc. Chem. Res.* **1986**, *19*, 138.
(2) Dagenais, M.; Downer, M.; Neumann, R.; Bloembergen, N. *Phys. Rev. Lett.* **1981**, *46*, 561. Downer, M. C.; Bivas, A.; Bloembergen, N. *Opt. Commun.* **1982**, *41*, 335. Downer, M. C.; Cordero-Montalvo, C. D.; Crosswhite, H. *Phys. Rev. B: Condens. Matter* **1983**, *B28*, 4931. Cordero-Montalvo, C. D.; Bloembergen, N. *Phys. Rev. B: Condens. Matter* **1984**, *B30*, 438. Cordero-Montalvo, C. D. *Phys. Rev. B: Condens. Matter* **1985**, *B31*, 6935.
(3) Payne, S. A.; Goldberg, A. B.; McClure, D. S. *J. Chem. Phys.* **1983**, *78*, 3688; *J. Chem. Phys.* **1984**, *81*, 1529. Chien, R. L. *Chem. Phys. Lett.* **1984**, *112*, 534. Chien, R. L.; Simonetti, J.; McClure, D. S. *J. Lumin.* **1984**, *31*, 326.
(4) Telle, H.; Huffer, W.; Basting, D. *Opt. Commun.* **1981**, *38*, 402.
(5) Chien, R. L.; Berg, J.; McClure, D. S. *J. Chem. Phys.* **1986**, *84*, 4168.
(6) Denning, R. G.; Snellgrove, T. R.; Woodwark, D. R. *Mol. Phys.* **1979**, *37*, 1109.
(7) Jørgensen, C. K.; Reisfeld, R. *Struct. Bonding (Berlin)* **1982**, *50*, 136.

0020-1669/87/1326-1721$01.50/0

Table I. Laser Dyes

dye	wavelength range, nm
IR-140	961–903
dibenzocyanin	947–900
hexacyanin 3	900–850
styryl-9	880–810
methyl DOTC	820–780
oxazine 750	790–750
nile blue	750–687
LD 700	745–685
DCM	690–615
sulpharhodamine 101	670–610
rhodamine 640	635–606
LD 700[a]	1029–971
DCM[a]	905–838
R590 (rhodamine 6G)[a]	720–746

[a] These dyes were used with Raman shifting.

rations of the linear unit are predominantly $\sigma_u\delta_u$ and $\sigma_u\phi_u$ in character,[6] while another is that $\pi_u{}^3\phi_u$ and $\pi_u{}^3\delta_u$ best describe the first excited states.[7] In both cases the spin–orbit interaction is a large and important feature in the pattern of the states. In either case the transitions are simplistically seen as excitations from orbitals primarily located on the oxygen atoms to uranium f orbitals although some recent relativistic calculations, with different levels of sophistication,[12,13] conclude that they are better described as one-center transitions on the uranium atom. In this paper we will present results that bear on this question. Because the $\pi^3\gamma$ configurations give a much larger number of excited states than the $\sigma\gamma$ configurations, it is important to be able to characterize all of the states and to be sure that none of them has evaded identification. The complexity of the OPA spectrum is such that extra states could easily be overlooked. In an earlier attempt to overcome this difficulty, we studied systems in which ligand substitution removes the center of symmetry, enhancing the intensity, in OPA, of the pure electronic transitions.[14] We shall show that by using the TPA spectrum the possibility that states have been overlooked can be much reduced and that regions of the spectrum can be probed which are opaque in OPA.

Experimental Section

Single-crystal samples were cut and oriented as previously described.[8] They were mounted in one of two continuous-flow liquid-helium optical cryostats (Oxford Instruments CF100 and CF204) at approximately 5 K. The cryostat was mounted in a light-tight box. The emitted light was passed through a broad-band interference filter with a half-width of 50 nm centered at 550 nm, which passes the strongest portion of the emission spectrum of $Cs_2UO_2Cl_4$, supplemented by green or blue transmission band color filters. The detectors were EMI photomultipliers, either Type 9816Q (S-20 photocathode) or Type 9813Q (S-1 photocathode). The latter tube has no sensitivity beyond 620 nm and is unaffected by the greater part of the spectral range of laser photon energies used in these experiments. Two laser systems were used: either a Lambda Physik FL2002 dye laser, pumped by an excimer laser (Lambda Physik EMG 150), or a Quantel Datachrom 5000 Nd-YAG pumped dye laser. The latter laser was also used with a Raman shifter using a single-pass 25-cm cell filled with approximately 50 bar of hydrogen. The first Stokes wave was selected by means of a prism. The laser dyes used in this work are listed in Table I.

A description of an experimental layout similar to that employed here can be found in ref 1b. The light incident on the sample consisted of pulses with typical energies in the 1–5-mJ range and with an optical bandwidth of 0.1–0.2 cm^{-1}. The beam was loosely focused with a 50 cm focal length lens through a small aperture, a 10-cm baffled tube, and a red-blocking filter. The combination of this filter and that covering the photomultiplier prevents the detection of any external light. The beam energy was monitored by a photodiode detector (Molectron, Type LP101). This detector monitors integrated pulse energies. Both the emission intensity and the reference pulse energy were recorded on a dual-channel transient digitizer (Biomation, Type 8100). Some data were also collected by using single-photon counting. The data were processed after being passed to a Research Machines 380Z microcomputer.[15] Data points in the immediate time proximity of the laser pulse were discarded from the digital record; they were affected both by the radio-frequency pickup accompanying the firing of the laser and by transients due to the detection of laser radiation. In some experiments artificial optical transients due to dielectric breakdown in the focused beam were observed and had to be discarded. In a typical experiment, with the transient digitizer, the time-integrated luminescence following each laser pulse was averaged over eight shots. This was scaled by the average of the square of the photodiode output for the same set of laser pulses. Strictly, the luminescence should be scaled in this fashion after every laser shot, and this was done for the data gathered by photon counting, but limitations on processing time required a compromise for the data taken from the transient digitizer. The shot to shot fluctuations in the luminescence intensity were typically 25% and are not sufficiently large for serious errors to arise in this way.

No attempt was made to eliminate the effects of transverse mode hopping, which can affect the measurement of reliable absolute intensities,[16] but the consistency of the relative intensities in repeated scans implies that random mode hopping is not significant. Because no use is made of small intensity differences in the spectrum, we have not monitored or corrected for changes in the dye laser pulse width with wavelength, which, by affecting the intensity–time profile, can introduce a source of error in the two-photon cross sections if the reference detector measures the integrated pulse energy.[16] The main effect of this omission arises from the narrowing of the pulses near the ends of the dye gain profile, where the lasing threshold is exceeded only near the peak of the pump laser pulse. The two-photon intensities at these points will be overestimated compared to those in the center of the dye range.

Using focused beams, we observe that the amplitude of the emission decays rapidly after the first few laser shots. Steering the beam onto another area of the sample temporarily restores the intensity, but it is apparent that the crystal surface is initially damaged by the focused beam. With the greater pulse energies of the Nd-YAG pumped dye laser and photon counting it is not necessary to focus the beam and there is no damage to the crystal, nor is there evidence of dielectric breakdown. We have investigated the linear polarization of most of the spectrum reported here, but the degree of polarization is not very reproducible, presumably because of depolarization and scattering. The depolarization can originate in the damaged areas of the crystal and also by the depolarization of beams reflected from the sample mount. In general, better polarizations were obtained by using a blackened mounting plate. When attempts are made to double-pass the beam by using a clean but unpolished brass mount, the polarizations are significantly poorer. Unfortunately, most of the data were collected on the latter type of mount. For this reason it is not possible to compare the absolute intensities of features in different polarizations, but their relative intensities are significant.

Identification of Excited States

The space group of $Cs_2UO_2Cl_4$, $C2/m$, is rigorously centrosymmetric with uranium atoms at positions of C_{2h} site symmetry. The crystal structure in relation to the crystalline habit has been described previously.[8] The spectroscopic data in one-photon absorption are conveniently described in terms of $D_{\infty h}$, D_{4h}, and D_{2h} symmetries. The cylindrical field provides the dominant perturbation; the tetragonal field, imposed by the chloride ions, is subject to a very small orthorhombic distortion. There are no spectroscopic features in OPA that require the use of C_{2h} symmetry to explain them.[9]

(8) Denning, R. G.; Snellgrove, T. R.; Woodwark, D. R. *Mol. Phys.* **1975**, *30*, 1819.
(9) Denning, R. G.; Snellgrove, T. R.; Woodwark, D. R. *Mol. Phys.* **1976**, *32*, 419.
(10) McGlynn, S. P.; Smith, J. K. *J. Mol. Spectrosc.* **1961**, *6*, 164. Newman, J. B. *J. Chem. Phys.* **1965**, *43*, 1691; **1967**, *47*, 85. Gorller-Walrand, C.; Vanquickenborne, L. G. *Spectrochim. Acta, Part A* **1972**, *28*, 257; *J. Chem. Phys.* **1972**, *57*, 1436. Brint, P.; McCaffery, A. J. *Mol. Phys.* **1973**, *25*, 311.
(11) Ellis, P. F.; Rosen, D. E.; Walch, P. F. *Int. J. Quantum Chem.* **1975**, *9*, 351. Walch, P. F.; Ellis, D. E. *J. Chem. Phys.* **1976**, *65*, 2387. Yang, C. Y.; Johnson, K. H.; Horsley, J. A. *J. Chem. Phys.* **1978**, *68*, 1000. Wadt, W. R. *J. Am. Chem. Soc.* **1981**, *103*, 6053. Tatsuumi, K.; Hoffmann, R. *Inorg. Chem.* **1980**, *19*, 2656. Boring, M.; Wood, J. H. *J. Chem. Phys.* **1979**, *71*, 392.
(12) Pyykko, P.; Lohr, L. L. *Inorg. Chem.* **1981**, *20*, 1950. Pyykko, P.; Laaksonen, L. *J. Phys. Chem.* **1984**, *88*, 4892.
(13) DeKock, R. L.; Baerends, E. J.; Boerrigter, P. M.; Snijders, J. G. *Chem. Phys. Lett.* **1984**, *105*, 308.
(14) Denning, R. G.; Norris, J. O. W.; Laing, P. J. *Mol. Phys.* **1985**, *54*, 713.
(15) Ironside, C. N.; Denning, R. G. *J. Phys. E* **1981**, *14*, 468.
(16) Birge, R. R. In *Ultrasensitive Laser Spectroscopy*; Kliger, D. S., Ed.; Academic: New York, 1983; p 109.

Table II. Polarization Selection Rules

electronic excited state								
sym			transition moments		polarizns of coupled vib (D_{2h})			
$D_{\infty h}$	D_{4h}	D_{2h}	OPA	TPA	A_g	B_{1g}	B_{2g}	B_{3g}
Σ_g^+	A_{1g}	A_g	$\theta_{3z^2-r^2}$	xx,[a]	xx,	xy	xz	yz
Σ_g^-	A_{2g}	B_{1g}	μ_z	xy	xy	xx,	yz	xz
Π_g	E_g	B_{3g}	μ_x,θ_{xz}	yz	yz	xz	xy	xx,
Π_g	E_g	B_{2g}	μ_y,θ_{yz}	xz	xz	yz	xx,	xy
Δ_g	B_{2g}	B_{1g}	θ_{xy}	xy	xy	xx,	yz	xz
Δ_g	B_{1g}	A_g	$\theta_{x^2-y^2}$	xx,	xx,	xy	yz	xz

[a] This notation indicates the set xx, yy, and zz.

The transition probability in two-photon absorption is proportional to

$$\sum_k \frac{|\langle j|\mathbf{r}_a|k\rangle\langle k|\mathbf{r}_b|a\rangle|^2}{\hbar^4(\omega - \omega_{ka})^2}$$

where a, j, and k label the ground, excited, and intermediate states respectively, ω is the frequency of the photon field, and ω_{ka} is the frequency of the virtual transitions that constitute the intermediate state. In the orthorhombic D_{2h} group, three linear dipolar polarizations are significant and there are six two-photon polarizations, which we describe by the products of the polarization vectors for the two photons: xx, yy, zz, xy, xz, and yz. These combinations give rise to a set of selection rules for the pure electronic transitions, which are summarized in Table II for the relevant symmetries. This table also shows the selection rules for vibronic states corresponding to the coupling of the gerade local modes of the complex ion. Light linearly polarized along the orthorhombic axes x, y, and z will excite states of A_g symmetry. Light propagating in the z direction polarized at 45° to the x and y axes will also excite xx- and yy-polarized two-photon transitions but with an intensity one-fourth that in the case of polarization parallel to these axes.

Because the symmetry is close to D_{4h}, it is to be expected that the xx and yy intensities will be very nearly equal; indeed, this is the experimental position for the x and y electric-dipole intensities in OPA.[9] The xy polarization should therefore exhibit A_g features whose intensity is half that in the xx or yy polarizations. The strong dichroism parallel and perpendicular to the z axis in OPA means that this is not a useful argument for the intensities in the xz and yz polarizations. Notice that excited states of B_{1g} symmetry should have zero intensity in the xx and yy polarizations but non-zero intensity in the xy polarization.

In the special case that an A_g, $B_{1g}(D_{2h})$ pair of states is derived from the first-order tetragonal field splitting of a $\Delta_g(D_{\infty h})$ state and that the wave functions are only slightly perturbed, we have the additional constraint expressed in D_{4h} symmetry that

$$\langle B_{2g}|\mathbf{m}_x|E_u(y)\rangle = \langle B_{1g}|\mathbf{m}_y|E_u(y)\rangle$$

so that, for example

$$\langle B_{2g}|\mathbf{m}_x|E_u(y)\rangle\langle E_u(y)|\mathbf{m}_y|A_{1g}\rangle = \langle B_{1g}|\mathbf{m}_y|E_u(y)\rangle\langle E_u(y)|\mathbf{m}_y|A_{1g}\rangle$$

where $\mathbf{m}_x$ and $\mathbf{m}_y$ are components of the electric-dipole operator. This result leads to the expectation that in the xy polarization the intensities of an A_g and $B_{1g}(D_{2h})$ pair of states related in this way should be approximately equal. When these results are taken with the reduction of the A_g features to half-intensity at the 45° position, we obtain the requirement that in cylindrical symmetry the absorption of the parent Δ_g states must be isotropic. A general analysis of polarizations in TPA has been made.[17]

Finally, notice from Table II that two-photon spectroscopy should be particularly helpful in identifying excited states that in OPA are only allowed by the electric-quadrupole mechanism and that are relatively difficult to observe and characterize. In particular the states with $\Delta_g(D_{\infty h})$ parentage, with the exception of one, for which an electric-quadrupole mechanism has been proven,[8] are not observed in OPA. In this one case the special polarization properties established the state symmetry, but otherwise the excited-state symmetries are based upon a potentially contentious assignment using the shape of vibronic sidebands.[9]

(17) Bader, T. R.; Gold, A. *Phys. Rev.* **1968**, *171*, 997.

Table III. Electronic State Parameters

origin	sym in D_{2h}	energy/cm^{-1}	polarizn OPA	polarizn TPA	vib freq/cm^{-1} ν_1	ν_{11}	ν_4
ground state	A_g				832	200/204	264
I	B_{2g}	20095.7	μ_y	xz	714.8	172/174.6	
II	B_{3g}	20097.3	μ_x	yz	714.6	172/174.6	
III	B_{1g}	20406.5	θ_{xy}	xy	710.3	178	265
IV	A_g	21316		xx, yy	696	175	262
V	B_{2g}	22026.1	μ_y	xz	712	147	268
VI	B_{3g}	22076			710	149	268
VII	A_g	22406		xx, yy	717		260
VIII	B_{1g}	22750		xy	711	173	265
IX	B_{2g}	26197.3	μ_y	xz	724.7	174	
X	B_{3g}	26247.6	μ_x	yz	724.3	174	
XI	B_{1g}	27719.6	μ_z	xy	705.4	170	
XII	A_g	27757		xx, yy	708	170	
XIII	A_g	29277		xx[a]	680 ± 3		
XIV	B_{1g}	29546		xy[a]	734 ± 5		

[a] Polarizations in this region are poorly defined.

Following the method established earlier,[9] we confirm the identity and origins of progressions in the O–U–O stretching modes from a comparison with the data from a crystal containing more than 98% oxygen-18. Origin bands shift typically 10 cm^{-1} to higher energy on isotopic substitution as a consequence of the difference in the ground- and excited-state zero-point vibrational frequencies. The mode numbering adopted here follows the D_{4h} scheme used in ref 9.

Results and Discussion

Figure 1 shows a survey of the complete TPA spectrum in the $Z(xy)$ polarization. This nomenclature describes an experiment in which the light propagates in the z direction and the polarization is linear and is directed at 45° to the x and y axes. The figure also shows the $X(y)$-polarized OPA for comparison. Within the range of a single laser dye the intensities have been divided by the square of the reference beam intensity. Different dye segments have been patched together, with intensities matched where possible in overlapping segments, in such a way as to make the Franck–Condon factors in progressions appear reasonable; so the relative intensity between segments has only limited significance. Note also the possibility of relative intensity distortions within the range of a single dye caused by the neglect of pulse width variations (see Experimental Section). In this spectrum B_{2g} and $B_{3g}(D_{2h})$ excited states appear weakly as a result of imperfect polarization.

Origin Bands. The TPA spectrum displays evidence of fourteen electronic excited states between 20000 and 32000 cm^{-1}. Thirteen origins are observed directly, and one is inferred from the vibronic structure built on it. The energies of these states are shown in Table III, which also indicates the polarizations of the origins in both OPA and TPA in those cases where any intensity is observed. The TPA data complement those from OPA, locating origins IV, VII, VIII, XII, XIII, and XIV directly. In our OPA analysis[9] the first four of these states were inferred from vibronic features while origins XIII and XIV were not detected.

Figure 1 shows that in the region of XIII and XIV OPA shows a broad, featureless absorption rising to shorter wavelength and reaching a flat cutoff at 29000 cm^{-1} in which the residual transmission represents stray light. The TPA shows little of this rising background, which must be due to a parity-changing transition, but reveals the underlying parity-conserving transitions.

Origins XIII and XIV are confirmed by their oxygen-18 isotope shifts of ~10 cm^{-1} to higher energy. The bands are then either the origins themselves or vibronic features in which oxygen motions are not involved. At first sight the interval between XIII and XIV, 269 cm^{-1}, is sufficiently close to the chlorine totally symmetric

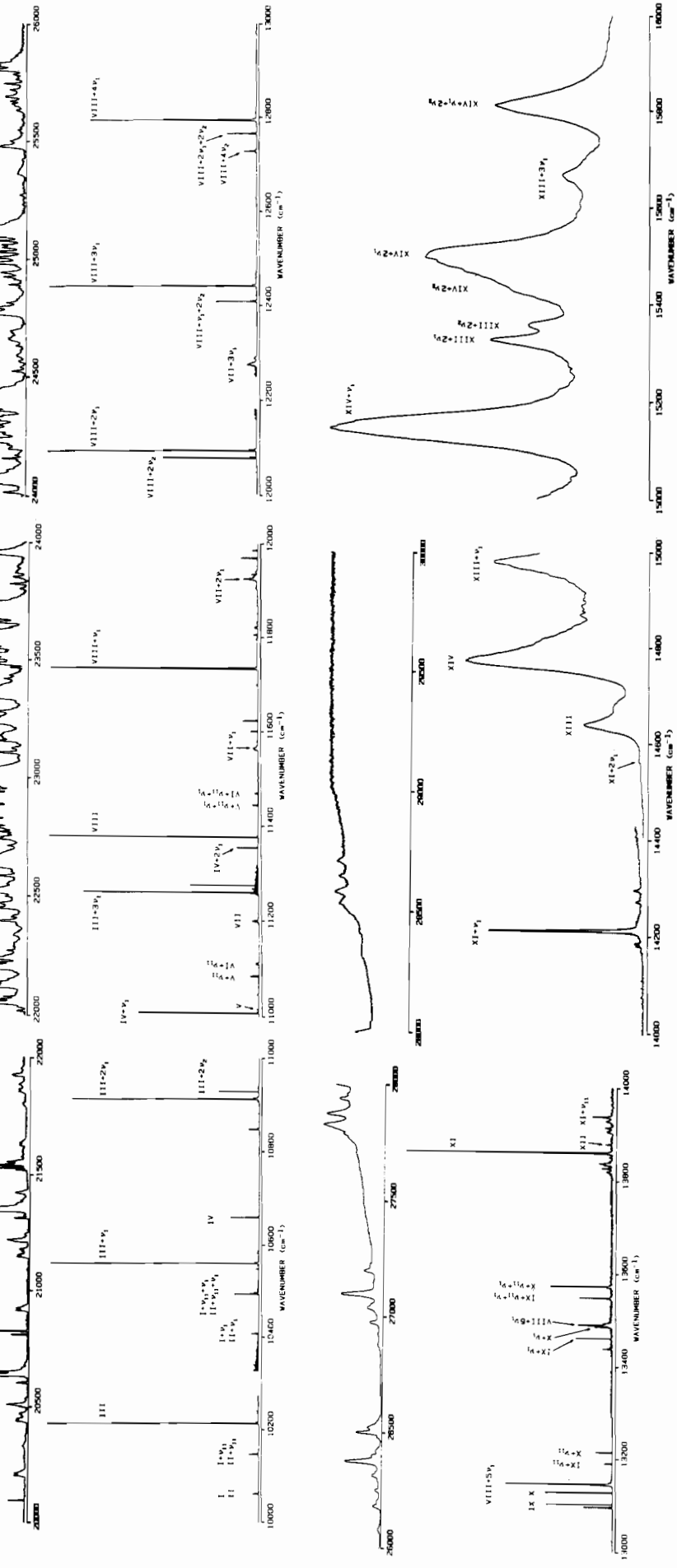

Figure 1. Single-crystal absorption spectra of $Cs_2UO_2Cl_4$ at 4.2 K. Segments between 11 000 and 16 000 cm^{-1} are TPA spectra in the $Z(xy)$ polarization. The corresponding OPA spectra in the $X(y)$ polarization are shown, where available, immediately above each TPA segment.

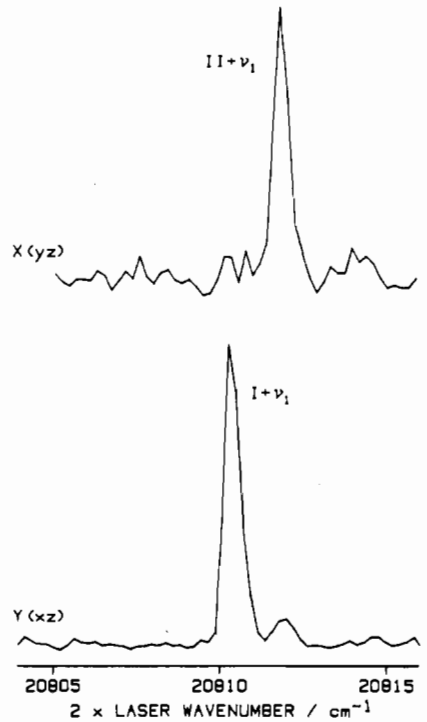

Figure 2. TPA spectra at 4.2 K in the *xz* and *yz* polarizations.

stretching frequency, ν_4, in the electronic ground state (see Table III) to suggest that the interval is a pure vibrational quantum. Two factors make this assignment untenable; first, the intensity ratio suggests that further members of a progression would be observed, but there is no evidence of this, and second, the vibrational interval in the O–U–O symmetric stretching progressions, 680 and 734 cm^{-1}, is quite different for these two bands. There is no evidence of appreciable anharmonic interaction between ν_1 and ν_4 in other transitions where they are both observed, and so the features at 29 277 and 29 546 cm^{-1} are interpreted as two separate electronic origins. Qualitatively these bands are easily the most intense features in TPA. The polarizations in this region, although poorly defined, imply that XIII and XIV have A_g and B_{1g} symmetries, respectively.

The large width of XIII and XIV is not unexpected. In OPA the spectrum becomes relatively broader above 26 000 cm^{-1} and starts to show a featureless rising background (see Figure 1). The presence of a broad underlying state is confirmed by the observation of a Fano antiresonance at 28 460 cm^{-1}.[9] The broadening of XIII and XIV is therefore interpreted as a rapid decay of these states into the underlying broad state. The latter probably arises from chloride to uranium charge transfer, because in the analogous bromide compound a comparable intense and broad absorption is found at much lower energy.[18] In the latter case this broad state appears to be responsible for the quenching of the luminescence at room temperature.

Figure 2 shows the polarization of origins I and II in the region of the spectrum where the absorption is due to the first member of the progression in the symmetric UO_2 stretch. The symmetry of these origins, which are separated by 1.6 cm^{-1}, is well-known from their magnetic-dipole polarizations in OPA.[8,9] This figure confirms the expected TPA polarizations (Table II), which in this example are almost complete. The symmetries of origins III, IV, VII, and VIII can be deduced from their relative intensities in the *xy* and *yy* polarizations. A typical spectral region showing the degree of polarization is presented in Figure 3. Although the polarization shown in the figure is not complete, it is sufficiently clear to confirm that both III, IV and VII, VIII constitute A_g, $B_{1g}(D_{2h})$ pairs of states stemming from the tetragonal field splitting of states of $\Delta_g(D_{\infty h})$ parentage in the cylindrical UO_2^{2+} ion. Notice

(18) Denning, R. G.; Ironside, C. N.; Snellgrove, T. R.; Thorne, J. R. G. *Mol. Phys.* **1982**, *47*, 443.

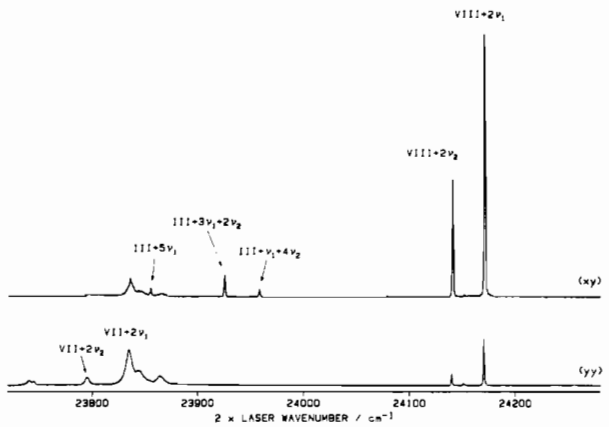

Figure 3. TPA spectra at 4.2 K in the *xy* and *yy* polarizations.

that this splitting is 910 cm^{-1} for origins III and IV but is 344 cm^{-1} and of inverted sign for origins VII and VIII. The significance of this inversion will be discussed later. Careful intensity measurements at fixed wavelength in the *xy* and *yy* polarizations give the ratios 1:1.95 for VII + $2\nu_1$ and 1:0.04 for VIII + $2\nu_1$. The expected ratios for A_g and B_{1g} excited states are 1:2.0 and 1:0.0.

Figure 3 also reveals a remarkable feature that is made clear by the relative simplicity of the TPA spectrum. Origin VII consists of broad absorption features that, in the case of the second member of the progression in the UO_2 symmetric stretch, shown in the figure, have a width of $\sim$10 cm^{-1}, compared with the typical widths of less than 1 cm^{-1} for the structure associated with the other low-energy electronic transitions.

All of the structure built on VII is broad, but the width of the origin of the progression appears to be narrower (4.5 cm^{-1}). The position of VII is confirmed by oxygen-18 substitution. It should be emphasized that the width of the electronic transitions is only detectable in TPA, the vibronic structure in OPA being subject to broadening by the vibrational dispersion. The large half-width can be attributed either to the dephasing due to a strong electron–phonon interaction or to rapid relaxation to a neighboring electronic state. The former hypothesis is unlikely because the wave function in this state should not have an orbital character significantly different from that of other states in the manifold. Nor is there evidence for a strong temperature dependence of the width, which would be anticipated for a phonon broadening mechanism. Instead we believe that the width is due to a strong coupling of VII to a lower electronic state by the vibrational Hamiltonian. It seems likely that the complex broad structure within this region represents a convolution of the underlying vibrational density of states built on lower energy origins and the vibrational coupling matrix elements. The interval between VII and IV, which shows the same, $A_g(D_{2h})$, electronic symmetry, is 1090 cm^{-1} while the intervals between VII and V and between VII and VI are 380 and 330 cm^{-1}, respectively. Superimposed upon the latter origins are single quanta of the b_{2g} and $b_{3g}(D_{2h})$ UO_2 rocking modes (ν_{11}, E_g in D_{4h}), with frequencies of 147 and 149 cm^{-1}, which give intense vibronic features with the same polarization and symmetry as VII.

We propose that these modes couple V and VI to VII and that it is this interaction which provides a mechanism for their vibronic intensity. This proposal is supported by the anomalously low frequencies of these modes, which in these states are 25 cm^{-1} less than in any other state (see Table III). These vibronic bands are 181 and 233 cm^{-1} below the nominal position of VII and are within the range of the low-frequency chlorine-based local modes, which span the range 105–264 cm^{-1} and which provide a region in which a high density of vibrational states can be expected. Later, when the pattern of the modes that couple strongly has been established, we will return to the analysis of the broad features surrounding VII.

Vibrational Structure. We now turn to the detailed form of the vibronic structure. If the true number of electronic transitions

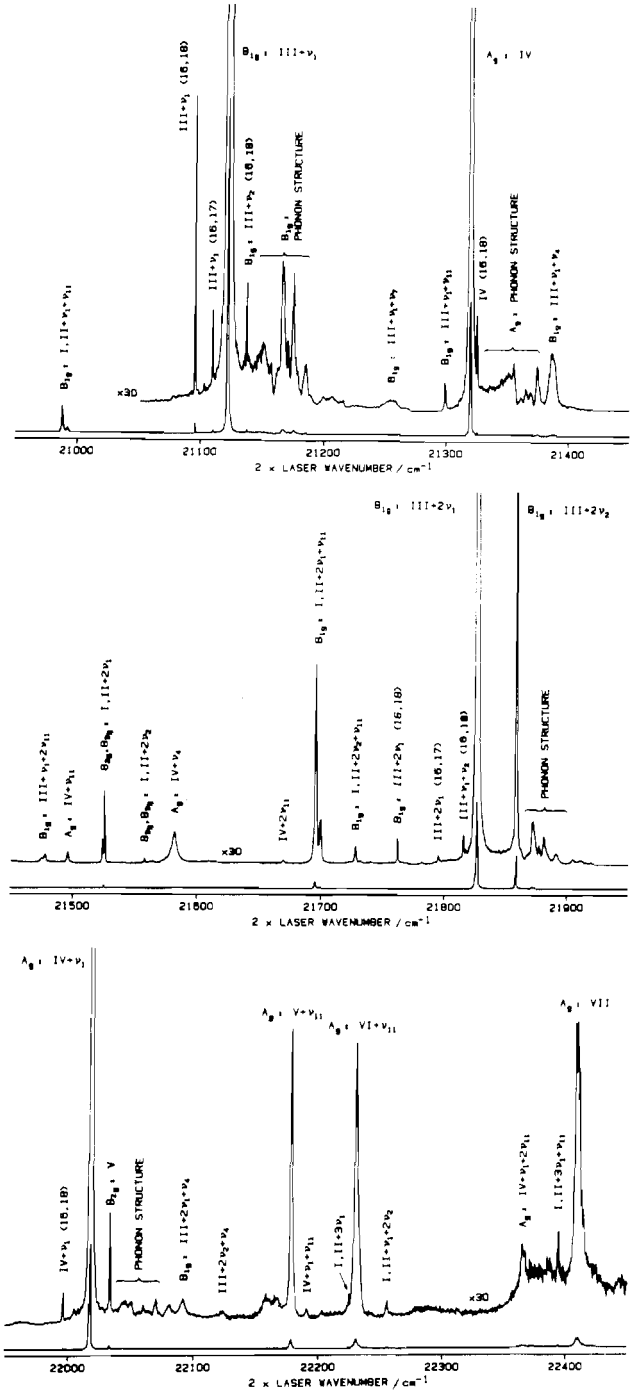

Figure 4. Single-crystal TPA spectrum at 4.2 K in an arbitrary, mixed polarization.

is to be found, it is essential to understand all the major vibronic features. To illustrate the extent to which the assignment can be made comprehensive, a single dye laser scan range is presented in Figure 4. This spectrum was taken on a large single crystal that had been deliberately oriented so that all possible two-photon transitions would be allowed. Comparison of this spectrum with the *yy*, *xy*, and *yz* spectra allows the excited-state symmetry of each feature to be determined unambiguously. These symmetries are shown in the figure.

In Figure 4 the TPA spectrum is shown as measured and is shown also with a 30-fold scale expansion. The features fall into two intensity categories. In the unexpanded spectrum the dominant bands are the electronic origins and progressions in the UO_2 symmetric stretch, ν_1, on those origins. At the second member of the progression on III, near 21 840 cm^{-1}, two sharp bands occur with a separation of 32 cm^{-1}, the higher energy component being weaker. We attribute the second band to the III + $2\nu_2$ vibronic state, which has the same total symmetry as III + $2\nu_1$ and which interacts with it through a large anharmonic coupling of the two stretching modes. Figure 1 shows the continuation of this progression with an identical splitting between III + $3\nu_1$ and III + $2\nu_2$ + ν_1. At the fourth member of the progression three bands are detected corresponding to III + $4\nu_1$, III + $2\nu_1$ + $2\nu_2$, and III + $4\nu_2$ with separations of 45 and 35 cm^{-1}, all of which have the same symmetry. The anomalous weakness of these features probably stems from the neglect of pulse width corrections, with the likely overestimation of the intensity of the previous component of the progression. The components of the fifth member of this series may be seen in Figure 3.

This same pattern occurs in the progression on origin VIII and is clearly visible in Figure 1. Indeed, most of the electronic states exhibit the same characteristics. It is particularly interesting that the broad progression on origin XIII exhibits the same pattern at its second member near 30 700 cm^{-1}. We were able to detect these multiple-component progressions in OPA for those origins with magnetic-dipole intensity.[9] The development of these multiple components, each of which can act as an origin for vibronic intensity in OPA, explains the way in which the complexity in OPA becomes intractable in the higher members of the progressions. However, the degree of detail available in TPA on the anharmonicity of the progressions is sufficient for further analysis of the anharmonic potential and will be reported in due course. A summary of the energies of the dominant vibronic progressions on all the origins is given in Table IV.

We now turn to the weaker features in Figure 4, most of which are labeled with their assignment in the figure. The correct assignment of these is important, given that the identities of the electronic configurations responsible for the states are best determined through the *number* of electronic states in this region of the spectrum (cf. Introduction). Accordingly, a rather detailed discussion follows illustrating the basis of these assignments and the level of our understanding of the spectrum. A general reader may wish to accept that the proper number of states has been determined and skip the remainder of this section.

The structure near 21 100 cm^{-1} illustrates the detail accompanying a single electronic transition. The bands at 21 091 and 21 105 cm^{-1} are due to the III + ν_1 transition in the isotopic species, which occur with a natural abundance of oxygen-18 and oxygen-17, respectively. In the UO_2^{2+} ion the main minority species present are designated (16,18) and 16,17), and the positions of their absorption features are in exact accord with their known isotope shifts.[9] The relative intensity of these bands is in agreement with their natural abundance ratio, 5.4:1, within the precision of the experiment.

The very sharp weak band at 21 132 cm^{-1} occurs at an energy identical with that of a very weak electric-dipole-allowed feature in OPA. It follows that the absorbing species lacks a center of symmetry. For this reason this feature is assigned to III + ν_2 in the (16,18) species. The two-photon intensity arises from the admixture of the ν_1 and ν_2 vibrations. This interaction also displaces their frequencies. From the position of the III + ν_1 band at 21 116.8 cm^{-1}, ν_1 has a frequency of 710.3 cm^{-1} in the (16,16) compound. The elementary effect of mass on this frequency predicts values of 683.0 and 669.7 cm^{-1} in the (18,16) and (18,18) ions, respectively. The observed values are 679.3 and 670 cm^{-1} so that there is a 3.7-cm^{-1} red shift in the (16,18) species from its expected position. We now allow for the interaction of ν_1 and ν_2 by diagonalizing an empirical matrix using a 12-cm^{-1} interaction between the two modes to describe their kinematic coupling. This gives the observed 41-cm^{-1} frequency separation and unperturbed values of 683.2 cm^{-1} for ν_1 and 716.2 cm^{-1} for ν_2. The latter value can be used to calculate a frequency of 727.7 cm^{-1} for this mode in the (16,16) species. This value is consistent with the frequency of $2\nu_2$ on origin III, 1446 cm^{-1}, when one remembers the presence of anharmonicity, and also with the values observed for ν_2 in OPA, which are 731, 729, and 727 cm^{-1} for origins I, II, and IX, respectively. This model then gives a consistent description of the frequencies of the two stretching modes in the (16,18) species. The eigenvectors predict that the TPA intensity ratio of ν_1 and

Table IV. Energies of the Principal Progression Bands (in cm^{-1})

origin	$+\nu_1$	$+2\nu_1$	$+2\nu_2$	$+3\nu_1$	$+2\nu_2 + \nu_1$	$+4\nu_1$	$+2\nu_1 + 2\nu_2$	$+4\nu_2$
I	20810	21520	21552					
I + ν_{11}	20983	21691	21723	22389				
II	20812	21522	21554					
II + ν_{11}	20987	21695	21728	23393				
III	21117	21821	21853	22516	22547	23196	23241	23276
IV	22012	22705	22735	23393	23434	24064	24114	24155
V + ν_{11}	22885	23580	23600					
VI + ν_{11}	22935	23629	23650					
VII	23123	23838	23798	24546	24472	25253	25197	
VIII	23461	24174	24144	24877	24812	25582	25525	25450
IX	26923	27655	27638	28372	28343			
IX + ν_{11}	27096	27829	27812	28545	28518			
X	26971	27702	27683	28418	28388			
X + ν_{11}	27145	27875	27858	28591				
XI	28425	29127						
XII	28465							
XIII	29957	30646	30707	31330	31397			
XIV	30280	30995	30880		31617			

origin	$+5\nu_1$	$+3\nu_1 + 2\nu_2$	$+\nu_1 + 4\nu_2$	$+4\nu_1 + 2\nu_2$	$+2\nu_2 + 4\nu_2$	$+6\nu_2$	$+6\nu_1$	$+7\nu_1$
III	23857	23927	23960	24610	24642			
IV	24704	24782	24835	25436	25493	25557		
VII	25957							27351
VIII	26283	26185		26878			26979	27674

ν_2 will be 9.5:1, which, considering the sharpness of the features, is in satisfactory agreement with the ratio of the observed peak heights of 4:1.

In the range from the origin at 21 117 to 21 180 cm^{-1} is a region of rising absorption with three main features at 48, 53, and 64 cm^{-1} from the origin. These intervals correspond well to bands in the Raman spectrum at 48, 53, and 69 cm^{-1} when it is recognized that the dispersion of the modes means that the Raman spectrum displays the spectrum at $\mathbf{k} = 0$ in the vibrational zone while the vibronic spectrum, conserving the total momentum, will show features that reflect the density of vibrational states. The upper limit of this region near 65 cm^{-1} is close to the Debye frequency of 58 cm^{-1} attributable to the acoustic modes. The latter value is derived from a study of the temperature dependence of the optical line-broadening and energy-transfer kinetics of this material.[19] An exactly analogous region of low-frequency phonon structure is observed on other origins, notably IV and VIII.

The broad band at 21 250 cm^{-1} has $B_{1g}(D_{2h})$ symmetry and is 133 cm^{-1} above origin III + ν_1. This interval clearly corresponds to the Raman band at 132 cm^{-1}, ν_7, which is due to a chlorine in-plane bending mode. This mode has $B_{1g}(D_{4h})$ or $A_g(D_{2h})$ symmetry so that its vibronic symmetry follows that of origin III, as observed.

The next sharp band at 21 295 cm^{-1} is 178 cm^{-1} above III + ν_1. Its repeat in the ν_1 progression, which is more clearly defined in the *xy*-polarized spectrum (not shown here), is at 22 000 cm^{-1}, an interval of 705 cm^{-1}. This strongly suggests that this feature is associated with III, for which the progression interval is 706 cm^{-1}, rather than I and II, or IV, for which the intervals are 709 and 696 cm^{-1}, respectively. The frequency of the mode corresponds well to those of the UO_2 rocking vibrations (see Table III) in other excited states. However, the *xy*-polarization of this feature gives it $B_{1g}(D_{2h})$ symmetry, which is incompatible with the b_{2g} and b_{3g} symmetry of these vibrations. Instead, the state appears to carry the same symmetry as the electronic transition. This can be understood by adopting the actual C_{2h} site symmetry, in which the rocking mode in the *xz* plane is totally symmetric. It follows that the excited-state equilibrium geometry of the ion has a small deformation with respect to the ground state in this coordinate. Examination of the crystal structure[20,21] shows that this deformation could be anticipated from the relatively short distances between the oxygen atoms and the cesium ions, which lie in the same mirror plane, and the notion that the transitions involve some transfer of charge from oxygen to uranium. There is evidence for a second member of a progression in this mode since a weaker band with the same polarization appears at 21 473 cm^{-1}, exactly 178 cm^{-1} above the first. It is accompanied by a small shoulder at 21 470 cm^{-1}, which may well correspond to the excitation of two quanta of the second rocking mode, giving a vibronic state that is also totally symmetric in C_{2h}. We conclude that the higher frequency of the two modes is totally symmetric in C_{2h} and so has b_{2g} symmetry in D_{2h}. The polarization of the rocking modes in the single-crystal Raman spectrum supports this sign for the orthorhombic splitting of these modes.[22]

This assignment is complemented by the presence of a similar sharp feature at 21 491 cm^{-1}, which is 175 cm^{-1} above IV and shares its polarization as an A_g excited state. There is also evidence for a second member of a progression in this case, at 21 666 cm^{-1}, with the identical 175-cm^{-1} interval. Equivalent sidebands can also be detected on origin VIII, where the interval is 173 cm^{-1}.

Origin IV is accompanied by a weak satellite 5 cm^{-1} to higher energy, which is due to the (16,18) isotopic species. The structure in the next 60 cm^{-1} is the now familiar acoustic phonon and lattice mode structure, which in this case has the same A_g symmetry as origin IV. However, the strong band at 21 382 cm^{-1} has B_{1g} polarization and is obviously built on III. The interval of 265 cm^{-1} clearly identifies this mode as the totally symmetric U–Cl stretching vibration with the notation ν_4, which has A_{1g} symmetry in D_{4h}.[9] The frequency is almost identical with the value of 264 cm^{-1} found in the Raman spectrum (taken at room temperature). This mode is found again coupled to IV, with the proper polarization, at 21 579 cm^{-1} with a frequency of 262 cm^{-1}. There is no evidence of progressions in this mode. We note that the chlorine modes display considerable width; for example, that at 21 579 cm^{-1} has a full-width half-maximum of $\sim$6 cm^{-1}. The shape of this feature, which tails to the red side, is comparable to the pattern expected for the natural abundance of chlorine isotopes. In a comparable case, where this isotope splitting is observed,[23] the separation between the five components is $\sim$2.1 cm^{-1}. The intensity of the three highest energy components is dominant, the ratios being 81:108:54:12:1, and the line shape in this instance is consistent with these values.

Continuing the analysis of Figure 4, the sharp bands at 21 520 cm^{-1} are due to I and II + $2\nu_1$ and are the next members in the progression after the bands shown in Figure 2. In a manner that will now be familiar, they are accompanied by weaker satellites

(19) Thorne, J. R. G.; Denning, R. G.; Barker, T. J.; Grimley, D. I. *J. Lumin.* **1985**, *34*, 147.
(20) Hall, D.; Rae, A. D.; Waters, T. N. *Acta Crystallogr.* **1966**, *20*, 160.
(21) Denning, R. G.; Ironside, C. N.; Thorne, J. R. G.; Woodwark, D. R. *Mol. Phys.* **1981**, *44*, 209.
(22) Ware, M. J., private communication.
(23) Tacon, R. J.; Day, P.; Denning, R. G. *J. Chem. Phys.* **1974**, *61*, 751.

32 cm^{-1} to higher energy, which are I and II + $2\nu_2$. The spectrum continues with two strong bands, both with the same B_{1g} polarization, at 21 691 and 21 695 cm^{-1}, which are obviously the rocking vibrations built on I and II + $2\nu_1$; the usual $2\nu_2$ satellites are found near 21 723 cm^{-1}. The polarization of these bands implies that the lower of them is due to the coupling of the b_{3g} vibration to origin I with B_{2g} symmetry and the upper of the two is due to the b_{2g} vibration on the B_{3g} state. The 4-cm^{-1} splitting is then the sum of the 1.6-cm^{-1} origin separation and a 2.4-cm^{-1} difference in the vibrational frequencies in the same sense as in the Raman spectrum. We note that the resultant vibronic symmetry is the same as that of origin III, from which the energy separation is only 133 cm^{-1}. There is no sign of the other possible vibronic bands with A_g symmetry arising, for example, from the coupling of the b_{2g} mode to the B_{2g} state. These extra bands should occur between those that are observed. Such a vibronic mechanism would need to draw intensity from the nearest electronic state with this symmetry, namely IV, which occurs 1050 cm^{-1} to higher energy.

The remainder of the spectrum in Figure 4 can be analyzed by using continuations of the structure that we have discussed above. For example, the bands at 21 760 and 21 792 cm^{-1} represent the continuation of the progression on origin III for the (16,18) and (16,17) isotopic species, respectively, while the band at 21 991 cm^{-1} is the next member on IV for the (16,18) species. Only the sharp band at 21 812 cm^{-1} presents difficulty. One possibility is III + ν_1 + ν_2 in the (16,18) species. Its separation from III + $2\nu_1$ is 52 cm^{-1}, somewhat larger than the 41-cm^{-1} separation between III + ν_1 and III + ν_2, but the influence of both anharmonic and kinematic coupling between the modes is difficult to quantify.

Finally, the spectrum above 22 000 cm^{-1} shows evidence for the presence of new electronic origins. The sharp band at 22 026 cm^{-1} is 14 cm^{-1} above IV + ν_1. By analogy with origin III a band due to IV + ν_2(16,18) should be observed near this frequency, but because the intensity of this feature is 3 times larger than that due to IV + ν_1(16,18) such an assignment is unsatisfactory. However, this position is exactly that at which OPA locates the magnetic-dipole-allowed origin V, and when the TPA spectrum of the (18,18) species is examined, a sharp band is found with the appropriate 10-cm^{-1} positive isotope shift from this energy. Although the polarization of this feature is not very well defined, it appears to be relatively more intense in the $Y(xz)$ polarization as anticipated for an electronic state with the B_{2g} symmetry expected for origin V (see Table II).

The two prominent features in the spectrum at 22 173 and 22 225 cm^{-1} are due to the b_{2g} and b_{3g} rocking modes on origins V and VI. The region near 22 400 cm^{-1} reveals the broad A_g origin VII, which we introduced earlier. Of particular interest is the broad band at 22 361 cm^{-1}. This absorption is 349 cm^{-1} from IV + ν_1, and we suggest that it is a repetition of the band ascribed to IV + $2\nu_{11}$ occurring at 21 665 cm^{-1}. Because it shares the same symmetry as VII and is only 45 cm^{-1} from it, we believe that there is a strong interaction between these states that contributes to their broadening and enhances the intensity of this feature. The best evidence for this assignment is that in the region where the next member of the ν_1 progression occurs on VII, at an interval of 712 cm^{-1}, the band that we have assigned to IV + $2\nu_1$ + $2\nu_{11}$ reappears with an interval of 696 cm^{-1}. The corresponding interval for the second member of the progression on IV is 693 cm^{-1}. We return to the structure surrounding VII in due course.

The purpose of this lengthy analysis is to show that every spectroscopic feature, including those whose intensity is less than $^1/_{200}$th of that of the largest bands, is identifiable in terms of either the local modes of the ion or acoustic and lattice modes. This is made possible by a dynamic range of at least 1000:1 in the experimental data. This point can be emphasized by observing the excellent definition of the band at 21 105 cm^{-1} in Figure 4, which is due to the natural 0.075% abundance of $U^{17}O^{16}O^{2+}$ in the crystal. There is no possibility that features in this intensity range could be attributed to additional excited states. Apart from the complication surrounding the vibronic interaction of both V and VI with VII, which we have already discussed, no new requirements are needed to explain the remainder of the structure in the sharp region of the spectrum below 29 000 cm^{-1}, every feature being attributable to the vibrational modes already encountered in Figure 4 in conjunction with the 12 electronic states in this region.

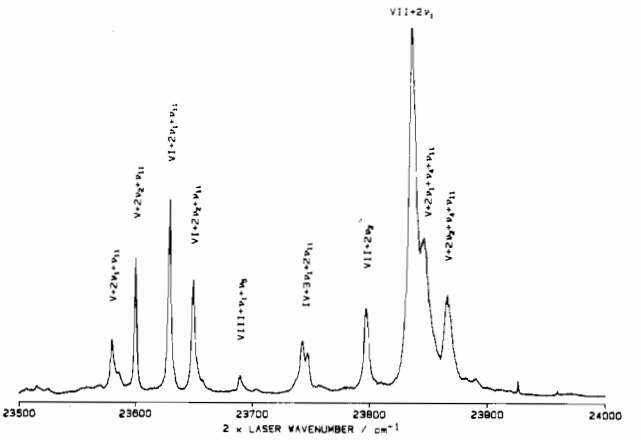

Figure 5. TPA spectrum at 4.2 K in the *yy* polarization.

We now return to the vibrational structure surrounding the broad absorption attributed to origin VII. When the progression in the UO_2 symmetric stretching mode reaches the second quantum, the structure surrounding the V and VI vibronic bands and VII becomes more complex (Figure 5). In contrast to other regions of the spectrum the portion between 23 500 and 24 000 cm^{-1} is superimposed upon a broad background. All the detail shown in Figure 5 shares the same *yy* polarization, implying A_g symmetry. The characteristic doubling due to $2\nu_1$ and $2\nu_2$ is seen in pairs of bands, with a 20-cm^{-1} separation, due to V and VI + ν_{11}. The origin of the interaction with VII is illustrated by the presence of two broad bands, with the same 20-cm^{-1} splitting, just above the absorption of origin VII itself, situated 268 cm^{-1} above the bands due to V + ν_{11}, an interval which we believe represents the chlorine stretching mode, ν_4.

On the low-energy side of VII + $2\nu_1$, at 23 690 cm^{-1} is a band due to VIII + ν_5 + ν_1, which occurs 229 cm^{-1} above VIII. The frequency of the ν_5 mode in the Raman spectrum is 230 cm^{-1}. The A_g vibronic symmetry of this band is consistent with the $B_{1g}(D_{2h})$ vibrational symmetry of this vibration. Also in this region is a pair of bands attributed to IV + $3\nu_1$ + $2\nu_{11}$, which are easily identified by their low progression interval and an appropriate isotope shift. The remaining band in this region is assigned to VII + $2\nu_2$. The oxygen isotope shift is correct for this assignment, which implies that in this state the $2\nu_2$ vibration is lower in energy than $2\nu_1$. While this order is inverse to that found in III and IV, it is the same order as found for origin VIII (as can be seen in Figures 1 and 3), which we believe to share the same cylindrical field parent state. The principles established in this portion of the spectrum can be confirmed in the region surrounding VII + ν_1 and are supported by the isotope shifts in that region. To summarize, although this part of the spectrum appears intractable, it is possible to explain all of the detail and the broadness in terms of the interaction of VII with the underlying vibrational levels built on other electronic states.

UO_2 Rocking Mode. The role of the UO_2 rocking mode is clearly important both in OPA, where it creates false origins,[9,24,25] and in the TPA spectrum, where it is principally present coupled to the $E_g(D_{4h})$ or B_{2g},$B_{3g}(D_{2h})$ origins, namely I, II, V, VI, IX, and X. The polarization behavior is different for each of these pairs of origins despite the formal symmetry of the states being identical in each case. This can occur because, for example, the b_{2g} vibration coupled to a B_{2g} electronic state can appear in the *yy* polarization while the b_{3g} vibration can give intensity in the

(24) Denning, R. G.; Foster, D. N. P.; Snellgrove, T. R.; Woodwark, D. R. *Mol. Phys.* **1979**, *37*, 1089.
(25) Denning, R. G.; Norris, J. O. W.; Brown, D. *Mol. Phys.* **1982**, *46*, 325, 287.

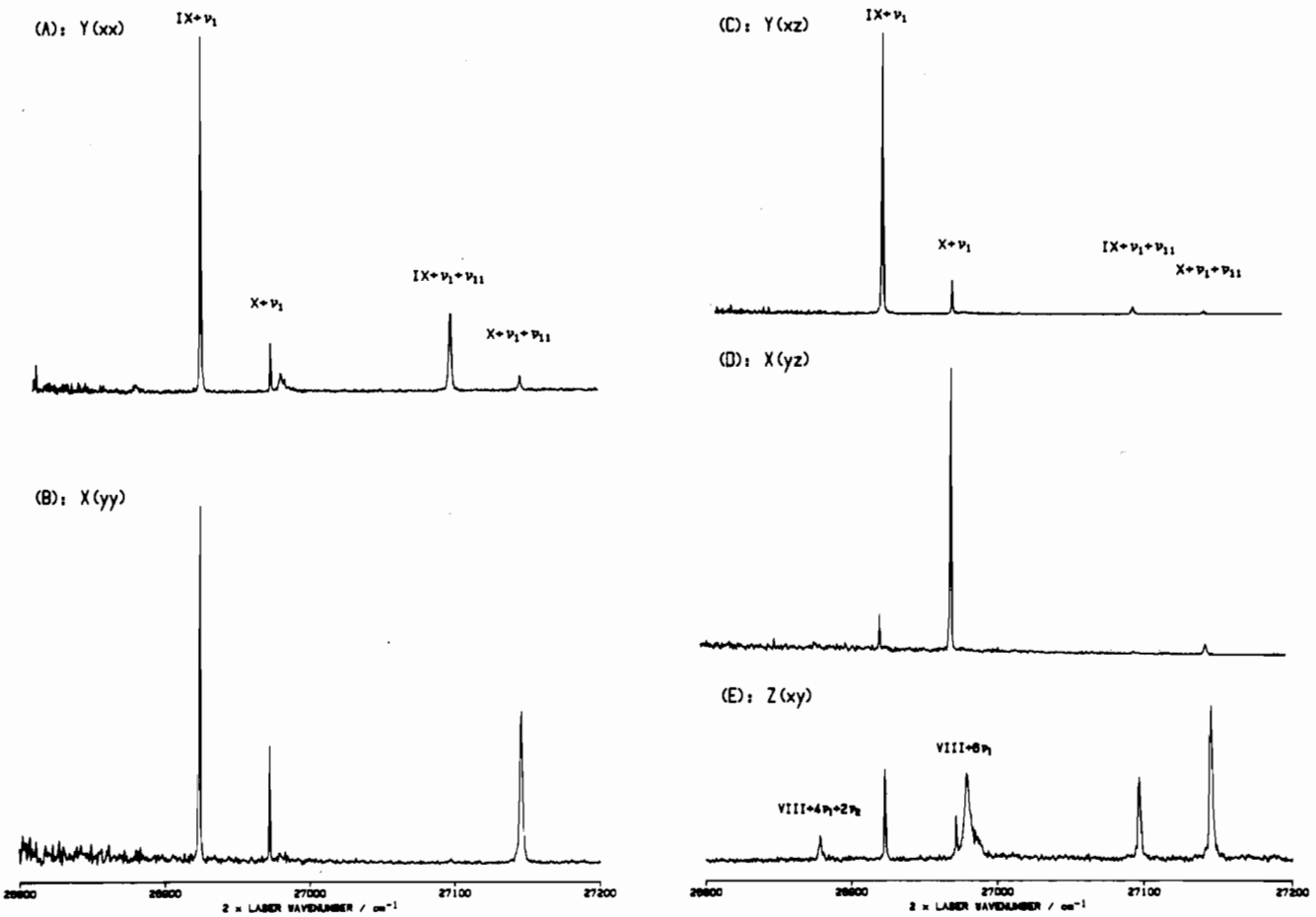

Figure 6. TPA spectra at 4.2 K in the *xx*, *yy*, *xz*, *yz*, and *xy* polarizations.

xy polarization. In practice origins I and II have sidebands with B_{1g} symmetry while those on origins V and VI have A_g symmetry. The simplest interpretation relies on the proximity of the nearby states. I and II are 305 cm^{-1} from III with B_{1g} symmetry but 1220 cm^{-1} from IV with A_g symmetry, while V and VI are 350 cm^{-1} from VII (A_g) but 700 cm^{-1} from VIII (B_{1g}).

The polarization of the sidebands due to these same vibrations on origins IX and X is quite different. The results of five different polarization experiments are shown in Figure 6. The absolute intensities in the five polarizations are not significant, and the appearance of IX + ν_1 and X + ν_1 in the *xx*, *yy*, and *xy* polarizations is a consequence of some depolarization (see Experimental Section). Despite these imperfections much can be learnt from these spectra. In a comparison of the *xx*, *yy*, and *xy* polarizations the obvious difference between them is due to the strong and broad band near 26 980 cm^{-1}, which is the sixth member of the progression in ν_1 based on origin VIII. This band is only significant in this polarization and has B_{1g} symmetry.

The most striking observation in the *xx* and *yy* spectra is the large difference in the intensities of the ν_{11} sidebands in the two polarizations. Indeed, a careful comparison between the *xx* and *xy* spectra shows some leakage of the *y* polarization into the former spectrum as shown by the presence of VIII + ν_1. It therefore seems likely that the intensity observed for X + ν_1 + ν_{11} in the *xx* spectrum is spurious and that the polarization of the sidebands between the *xx* and *yy* experiments is virtually complete.

When the intensity of these features is compared with that in the *xy*-polarized spectrum, both of these bands clearly behave in the manner expected of excited states with $A_g(D_{2h})$ symmetry so that the difference in their intensities in the two polarizations is unexpected. Remembering that the two components of ν_{11} have b_{2g} and b_{3g} symmetry, it is possible to explain the *xy* intensity of the sidebands as a projection of these *xx* and *yy* polarizations, in which case only the b_{2g} vibration is active on the B_{2g} origin (IX), while only the b_{3g} vibration is active on the B_{3g} origin (X). However, some of the *xy*-polarized intensity could be due to B_{1g} transitions induced by the second component of the rocking mode.

It appears hard to reconcile the remarkable intensity difference between the sideband intensities in the *xx* and *yy* experiments with the small departure from D_{4h} symmetry. In drawing intensity from A_g states the role of the b_{2g} vibration acting on IX would have been expected to be identical with that of the b_{3g} vibration acting on X. The 50-cm^{-1} separation between these states is small compared to the interval of 1500 cm^{-1} that separates them from the nearest states, XI and XII, and compared to their interval of 3000 cm^{-1} from XIII and XIV; the latter represent the closest states with large two-photon cross sections, from which the sideband intensity might be derived. In D_{4h} symmetry the relevant matrix elements have the form $\langle E_g(x)|E_g(x)|A_{1g}\rangle$ and $\langle E_g(y)|E_g(y)|A_{1g}\rangle$. There seems to be no satisfactory reason to anticipate any large difference between these interactions, so that intensity derived by this mechanism should be available to both sidebands in both the *xx* and *yy* polarizations.

To deal with this paradox, we turn to the hypothesis that the vibronic mechanism operates in the intermediate, nonstationary, state created by the photon field. First consider the *yy* polarization. If the electric-dipole operator is represented by $\mathbf{m}_y$ and the final A_g vibronic states are shown as the product functions $|B_{3g},b_{3g}\rangle$ and $|B_{2g},b_{2g}\rangle$, the transition probabilities are proportional to

$$\left|\frac{\langle A_g|\mathbf{m}_y|B_{2u}\rangle\langle B_{2u}|V(b_{3g})|B_{1u},b_{3g}\rangle\langle B_{1u},b_{3g}|\mathbf{m}_y|B_{3g},b_{3g}\rangle}{\Delta E(B_{2u},A_g)\ \Delta E(B_{2u},B_{1u})}\right|^2 \quad \text{(I)}$$

$$\left|\frac{\langle A_g|\mathbf{m}_y|B_{2u}\rangle\langle B_{2u}|V(b_{2g})|A_u,b_{2g}\rangle\langle A_u,b_{2g}|\mathbf{m}_y|B_{2g},b_{2g}\rangle}{\Delta E(B_{2u},A_g)\ \Delta E(B_{2u},A_u)}\right|^2 \quad \text{(II)}$$

where the operators $V(b_{2,3g})$ indicate the electronic–vibrational coupling. The intensity mechanism for the two electronic states now reflects the difference in these vibrational–electronic coupling matrix elements *in the intermediate state.*

It will become clearer why these elements should differ in magnitude if we make some assumptions about the electron configurations. Following our model of the electronic structure,[6] the electron is excited from a $\sigma_u(D_{\infty h})$ orbital having b_{1u} symmetry in D_{2h}. The B_{2u} intermediate state in expressions I and II then requires a one-electron excitation to a b_{3g} orbital. Within an elementary basis set this corresponds to the antibonding combination of the oxygen π_y orbitals and the $6d_{yz}$ orbital. The b_{3g} vibration describes a rocking of the UO_2 group in the yz plane and clearly provides a perturbation that is effective in mixing the $d_{yz}(b_{3g})$ orbital with the $d_{z^2}(a_g)$ orbital or molecular orbitals of the same symmetry; both component orbitals are involved in the uranium–oxygen bond. On the other hand, the b_{2g} rock occurs in the orthogonal plane and can, in principle, mix the $d_{yz}(b_{3g})$ and $d_{xy}(b_{1g})$ orbitals. However, in the equilibrium geometry, the latter orbital is excluded by symmetry from interaction with oxygen orbitals. It is then qualitatively clear that the oxygen motions do not provide an effective mechanism for coupling these orbitals when compared to the interaction, induced by the b_{3g} component of the mode, between d orbitals that both contribute to the oxygen bonding.

In this way it is easy to understand the asymmetry in the role of the two modes as a source of intensity with respect to any one electronic state. The same hypothesis, that the vibronic coupling occurs predominantly between orbitals that can form a bond to the displaced atoms, was advanced to explain the distribution of vibronic intensity in OPA.[6]

Because of this asymmetry and the fact that the polarization of the photon field prepares the B_{2u} intermediate state, only the b_{3g} vibration is effective in providing intensity in the yy polarization on the B_{3g} origin, X (expression I). An identical argument leads to the conclusion that the xx polarization should only display intensity through the b_{2g} vibration coupling to the B_{2g} origin, IX. Expression I shows that the same vibronic selectivity will lead to the occurrence of intensity in the xy polarization for both electronic states through the influence of either of the components of the mode because of the presence of both polarization components in the radiation field. Unfortunately, we are unable to distinguish experimentally between genuine xy polarization and the superposition of the xx and yy polarizations in this experiment.

Electronic Structure

The TPA spectra make the assignment of the electronic excited states in the range from 20000 to 32000 cm^{-1} almost unambiguous in their symmetry. The dynamic range of intensities and the extent to which the weak vibronic features can be analyzed make the probability that there are further unobserved electronic states in this region very low.

The most striking result of the vibronic analysis is that the uranium–chlorine vibrational frequencies are effectively identical in both the ground and excited electronic states. On the other hand, the oxygen stretching and rocking modes are both substantially weakened in the excited state. It is apparent from the electronic spectrum[6-10] that the interaction of the equatorial ligands with the valence orbitals of the uranium atom is not large, so that the chlorines may be viewed as bound in a manner that is largely ionic. If this is true, then the absence of any change in the uranium–chlorine symmetric stretching frequency in the excited states implies that there can only be a small oxygen to uranium charge transfer accompanying the excitation. This result provides experimental support for the conclusions of calculations by Pyykko et al.,[12] who find the HOMO to have about 80% uranium character, and DeKock et al., who find 79.6% uranium character.[13] Nevertheless, the refinement introduced by the latter authors, who included the fluorine valence orbitals of the $UO_2F_4^{2-}$ ion, seems untenable in this context. The result of the inclusion of the fluorines is to reduce the uranium content of the HOMO to 25% uranium character but to add 65% fluorine character to this orbital.[13] If this were the case in the analogous $UO_2Cl_4^{2-}$ ion, a large change would be expected in the uranium–chlorine stretch, as well as the appearance of a progression in this mode, on excitation to the LUMO, which all models view as heavily uranium-centered. DeKock et al. point out that this aspect of their calculation may be an artifact attributable to the neglect of the influence of the surrounding cation field on the energies of the fluorine orbitals.[13] In view of our results the calculation does seem defective in this regard.

An important feature of the work of DeKock et al. is that the relative orbital energies are strongly influenced by the change in the effective core potential that is introduced when the large relativistic effects are included as perturbations to the nonrelativistic Hamiltonian. The effect is to destabilize orbitals with large f character in relation to all others. The relative f-orbital energies are then partly controlled, through this effect, by the extent to which their f-orbital character is diluted by covalency. This has particular importance for the f_δ orbitals in the tetragonal environment of the ligands because the b_{2u} orbital[27] is required by symmetry to be nonbonding, while the b_{1u} orbital has a π-type interaction with the ligands. The combined effect of this dilution of the f-orbital character and the relativistic shift *destabilizes* the b_{2u} orbital, which has 100% f character, in relation to the b_{1u} orbital. The effect is to emphasize the tetragonal field splitting of the f_δ orbitals, but more importantly, the *sign* of this splitting is the opposite of that anticipated from a simple covalency model in which the *nonbonding* f_δ orbital would be expected to have the lower energy.

The experimental spectrum provides a test of the sign of this splitting, which is manifest in the splitting of $\Delta_g(D_{\infty h})$ states derived from coupling the excited f_δ electron to the electron remaining in the σ_u HOMO. In the Λ–Σ coupling scheme both singlet and triplet excited states arise and it is easy to show that these have opposite signs for their tetragonal field splitting (see ref 6, sections 5 and 6). With the confirmation available from TPA polarizations, origins III and IV, which have predominant triplet character,[6] place the $B_{2g}(D_{4h})$ component below the $B_{1g}(D_{4h})$ component. In the mainly singlet states XIII and XIV, the reverse ordering is observed. The latter order is that of the one-electron orbital energies, so that the observed order of the levels places the b_{2u} orbital below the b_{1u} orbital. This order is that expected on simple covalency grounds but is *not* that predicted by the relativistic model of DeKock et al. (remembering that the axis system used by these authors requires symmetry labels different from those used here). We therefore take the view that the model used by these authors may be defective.

The identification of two additional excited states, XIII and XIV, invites an attempt to refine the empirical model of the excited configurations that was used to account for the OPA spectrum.[6] The frequency of the UO_2 stretching mode in these states is sufficiently close to those in the remainder of the manifold to suggest that they arise from the same kind of configuration. Also the strong intensity in TPA suggests a mechanism related to that responsible for the strongest bands in the rest of the spectrum, in which case the states would be assigned $\Delta_g(D_{\infty h})$ symmetry. This view fits well with the expectation of two tetragonal field components that could be assigned to the two observed origins. The two-configuration model used previously does anticipate a $\Delta_g(D_{\infty h})$ state at approximately this energy.[6] Unfortunately, the degree of polarization that we observe in this portion of the spectrum is poor. Nevertheless, it seems clear that the higher energy component is relatively more intense in the xy polarization and so is assigned B_{1g} symmetry in Table III.

Since our earlier study of the uranyl ion[6] we have obtained independent data on the parameters governing the f electrons from study of the NpO_2^{2+} ion.[25] In this species a single electron occupies the f orbitals, and the optical spectrum reveals the relative energies of the f_ϕ, f_δ, and f_π orbitals. These energy differences may be used, with due attention to the electron–electron repulsion energies, to locate the approximate energy of the $\sigma\pi$ configuration in relation to the $\sigma\phi$ and $\sigma\delta$ configurations. To do this, we make use of the large one-center character of the optical transitions.[12,13] On the assumption that only the σ orbital has significant ligand character, the relative values of the electron–electron repulsion integrals can be expected to reflect the ratio of the one-center contributions (cf. ref 6, section 8.2).

The difference in these parameters for the various excited configurations determines the configuration energies in relation to the one-electron orbital energies, obtained from the spectrum of the neptunyl ion.[25] We obtain

$$J_{\sigma\phi} - J_{\sigma\delta} = -20F_2 + 60F_4 - 140F_6 = -12.2F_2'$$

$$J_{\sigma\phi} - J_{\sigma\pi} = -32F_2 + 12F_4 + 280F_6 = -24.0F_2'$$

$$K_{\sigma\phi} - K_{\sigma\delta} = -20F_2 + 60F_4 - 140F_6 = -12.2F_2'$$

$$K_{\sigma\phi} - K_{\sigma\pi} = -2F_2 + 48F_4 - 266F_6 = 0.9F_2'$$

where the definition of F_2' assumes the ratio of F_2, F_4, and F_6 that is observed to account for the states of the UCl_6^{2-} ion.[6] In the present case we use the value of $K_{\sigma\delta}$, 2900 cm^{-1}, which gives a good description of the spectrum in the region of the $\sigma\delta$ configuration, and its one-center definition, $20F_2 + 3F_4 + 224F_6 = 25.2F_2'$, to obtain $F_2' = 115$ cm^{-1}. The mean configuration energy differences are then given by

$$W_{\sigma\phi} - W_{\sigma\gamma} = (\epsilon_\phi - \epsilon_\gamma) - \{(J_{\sigma\phi} - J_{\sigma\gamma}) - (K_{\sigma\phi} - K_{\sigma\gamma})\}$$

where $\gamma = \delta$ or π. When $\gamma = \delta$, the exchange and Coulomb terms cancel and we can use the value of $\epsilon_\phi - \epsilon_\delta$, 1932 cm^{-1}, which is very well determined for $Cs_2NpO_2Cl_4$,[25] as a guide to the value for the difference in the configuration energies, $W_{\sigma\phi} - W_{\sigma\delta}$, in the uranyl case. When $\gamma = \pi$, the energy of the $\sigma\pi$ configuration, in wavenumbers, is given by

$$W_{\sigma\phi} - W_{\sigma\pi} = (\epsilon_\phi - \epsilon_\pi) - 2860$$

In the neptunyl ion $\epsilon_\phi - \epsilon_\pi = -13\,000$ cm^{-1}, so that the $\sigma\pi$ configuration can be estimated to lie $\sim 15\,000$ cm^{-1} above the $\sigma\phi$ configuration. The use of a one-center approximation will underestimate this difference, because the π orbital, unlike the δ and π orbitals, has some oxygen character. The one-center contribution to the electron–electron repulsion on oxygen has been ignored. On the other hand, the use of one-electron orbital energies taken from the NpO_2^{2+} ion may overestimate the equivalent energy differences in the uranyl ion, in which the metal–oxygen distance is longer. Evidently the $\sigma\phi$, $\sigma\pi$ separation will be on the order of 15 000 cm^{-1}.

Figure 7 shows the results of an empirical calculation of the type described previously,[6] but which includes the $\sigma\pi$ configuration. The states from this configuration are not shown in the figure because they are well above the energy range of the observed states. The diagram traces the evolution of the excited-state energies from initial states in which only the configuration energies and the spin–orbit interaction have been included. The subsequent stages show the inclusion of the electron–electron repulsion and the tetragonal field sequentially. Rather satisfactory agreement is obtained between the model and the observed energies. In particular the calculation reproduces the sign of the tetragonal splitting of origins III, IV and VII, VIII, whose ordering is unequivocally determined by the TPA polarizations. The source of the inversion of the sign of the splitting in these two pairs of states has been pointed out previously.[6]

The eigenvectors permit a calculation of the excited-state magnetic moments, which are in excellent agreement with those observed[9] and which are included in Figure 7. Similarly, it is possible to compute the relative intensity of the origin bands in both OPA and TPA, within groups of origins with the same D_{4h} symmetry. The calculation satisfactorily predicts the very weak intensity of origins V and VI, which are difficult to observe in both OPA and TPA. Qualitatively, this is a consequence of the important role of the $\sigma\phi$ configuration in these states which is not linked by the spin–orbit interaction with the $\sigma\pi$ manifold from which the intensity arises.

It is particularly interesting that the inclusion of the $\sigma\pi$ excited configuration resolves a difficulty in the ordering of the energy levels near 28 000 cm^{-1}, where the two-configuration model predicts[6] that the Δ states with $\sigma\delta_{5/2}$ parentage lie below the Γ state with $\sigma\phi_{7/2}$ parentage. As a result of the spin–orbit interaction, inclusion of the $\sigma\pi$ configuration forces down the low-energy Π and Δ states from the $\sigma\delta_{3/2}$ configuration with the result

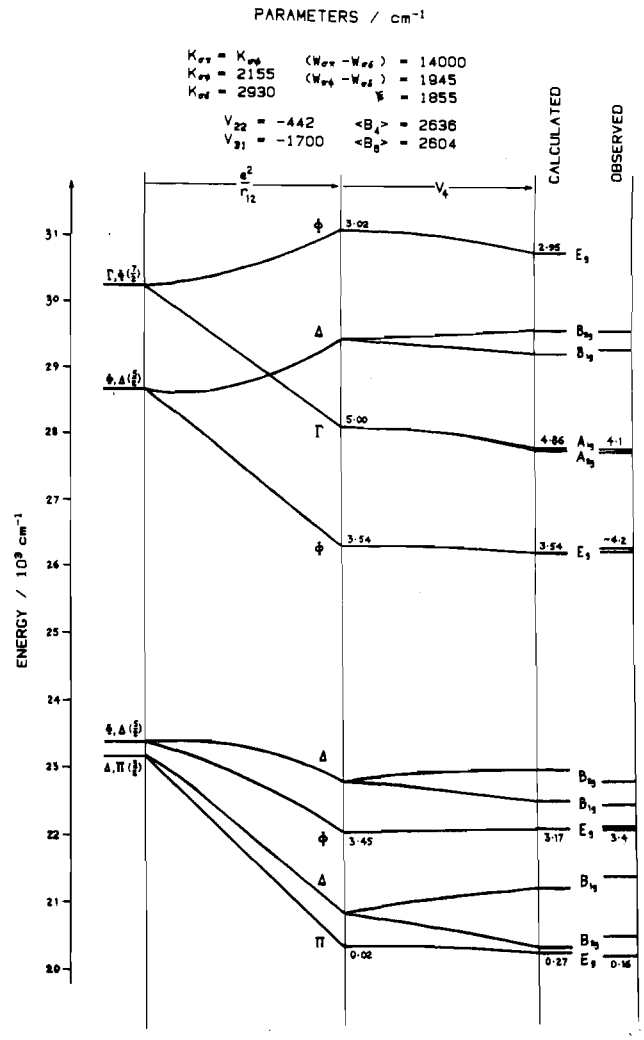

Figure 7. Calculated and observed energy levels of $Cs_2UO_2Cl_4$. The symmetries indicated at the right of the diagram are in D_{4h}. The numbers associated with the energy levels are magnetic moments in Bohr magnetons.

that the ϕ–δ separation can be reduced to a value comparable to that found in the neptunyl ion. This change and the increase in the electron–electron repulsion parameters that flow from it have the effect of raising the states arising from the $\sigma\delta_{5/2}$ configuration in relation to those from the $\sigma\phi_{7/2}$ configuration, thereby modeling the observed order of the levels.

The unsatisfactory ordering of these levels in our earlier two-configuration model has also been discussed in the work of DeKock et al.,[13] who showed that it could be remedied by introducing a much larger effective tetragonal field splitting, the source of which these workers attributed to differential relativistic stabilization. For the reasons set out above, we do not believe that the method of these workers gives a proper description of this splitting.

Conclusions

We believe that the discussion in the previous section makes the description of the dominant $D_{\infty h}$ configurations in this region of the spectrum as $\sigma\delta$ and $\sigma\phi$ unequivocal. Beyond these electronic structural implications the role of the UO_2 rocking mode, as illustrated in the TPA spectrum, deserves comment. The remarkable distribution of TPA polarizations for this mode on origins IX and X supports the view that the intensity mechanism is determined in the intermediate state. While this is the first example of vibronic intensity enabled in this way, it is not uncommon for perturbations active in the intermediate state to appear in the spectrum. In the TPA spectra of a variety of lanthanide ions the detailed interpretation of the polarizations requires the participation of spin–orbit and crystal field perturbations in the intermediate states which arise from $f^{n-1}d$ config-

urations.[26] We propose that an equivalent mechanism operates in the uranyl ion because, following the magnitudes of the static ligand fields, a much larger electron–phonon coupling should apply to the 6d orbitals, which constitute the intermediate states, as compared to that which applies to the 5f orbitals.

The TPA mechanism for the uranyl ion is then seen as two one-electron processes. The generation of the intermediate state corresponds to the $f_\sigma \rightarrow d_\pi$ transition. The same excited configuration is the source of the vibronic intensity in OPA. We note that this transition is polarized perpendicular to the UO_2 axis. The very strong linear dichroism in OPA indicates that the $f_\sigma \rightarrow d_\sigma$ transition occurs at much higher energies, as a result of the strong antibonding character of the d_σ orbital. In this model the second photon serves to complete the TPA transition through the $d_\pi \rightarrow f_\delta$ or $d_\pi \rightarrow f_\pi$ processes, depending on whether the polariation is y or z, respectively. It is now clear why the TPA intensity is dominated by the $\Delta_g(D_{\infty h})$ states which derive their intensity from the $\sigma\delta$ configuration. Moreover, this intensity will be largest in those states that have the largest singlet character. In our model calculations XIII and XIV have the largest singlet character and consequently relatively large transition probabilities. Qualitatively these states show by far the largest TPA intensity.

The much weaker TPA intensity in the xz and yz polarizations is a consequence of the relatively small role played by the $\sigma\pi$ configuration in the observed manifold. The spectrum of the neptunyl(VI) ion reveals that this configuration is approximately 15 000 cm^{-1} above $\sigma\delta$ and $\sigma\phi$,[25] and its contribution to the TPA intensity is then a second-order effect. The presence of this configuration must also be responsible for the x- and y-polarized magnetic-dipole intensity in OPA, and indeed the distribution of TPA intensity in origins I, II, V, VI, IX, and X closely follows the magnetic-dipole intensity in OPA.

Acknowledgment. We are indebted to the Science and Engineering Research Council for the support of T.J.B. and J.R.G.T. and to the staff of the Laser Support Facility at the Rutherford Appleton Laboratory for invaluable assistance.

(26) Bloembergen, N. *J. Lumin.* **1984**, *31–2*, 23.
(27) The notation used here differs from that in ref 13 because, throughout our work, we use an axis system that bisects the UCl_2 bond angles whereas DeKock et al. use axes that coincide with the U–Cl bonds.

Contribution from the Department of Chemistry,
Rice University, Houston, Texas 77251

Stoichiometry and Kinetics for Reactions of Tris(4,7-dihydroxy-1,10-phenanthroline)iron(II) with Oxygen, Hydrogen Peroxide, and Cyanide

Doan Trang Vu and David M. Stanbury*

Received October 21, 1986

$Fe^{II}(OHP)_3$ (OHP = 4,7-dihydroxy-1,10-phenanthroline) reacts with O_2 rapidly in alkaline aqueous solution. A major product of the reaction is HO_2^-; O_2^- is a feasible intermediate in the reaction. $Fe^{II}(OHP)_3$ reacts with HO_2^- to produce a 1:1 mixture of $Fe^{III}(OHP)_3$ and "$Fe^{III}(OHP)_2(OH)$"; this reaction has a rate law that is first order in [$Fe^{II}(OHP)_3$] but zero order in [peroxide], with a rate constant of 1.8×10^{-2} s^{-1} at 22 °C, pH 13. The substitution reaction of $Fe^{II}(OHP)_3$ with CN^- has the same rate law as the redox reaction with HO_2^- and a rate constant of 8×10^{-3} s^{-1}. Both the redox reaction of HO_2^- and the substitution reaction of CN^- are interpreted as having loss of the ligand OHP as the rate-limiting step. A sensitive and specific HPLC method has been developed for determination of HO_2^- in complex mixtures.

Introduction

The ligand 4,7-dihydroxy-1,10-phenanthroline (OHP), which is used as a reagent for iron in alkaline media, is quite unusual among the phenanthrolines.[1] The iron(III)–tris complexes of most phenanthrolines are well-known as a graded series of substitution-inert one-electron oxidants that are stable only in acidic media; however, $Fe^{II}(OHP)_3$ is stable only in alkaline media, and it is a strong reducing agent. At pH 13 the hydroxo groups are fully deprotonated, rendering the ligand a dianion. But the unusual nature of $Fe^{II}(OHP)_3$ cannot be ascribed simply to a charge effect, since the comparable sulfonated complexes fall in the class of the normal phenanthroline complexes. Apparently an unusual type of conjugation occurs when OHP is complexed as its dianion, which leads to a very strong affinity for Fe(III).

The reaction chemistry of $Fe^{II}(OHP)_3$ has not been extensively explored, probably because of difficulties in handling. The complex is very sensitive to O_2, and the free ligand is difficult to purify because it is resistant to sublimation and insoluble in all solvents except strong acids and bases. There is a fascinating report of the kinetics of the reductions of O_2 and HO_2^- by the complex; the O_2 reaction was reported to proceed with simple bimolecular kinetics but without the intermediacy of free O_2^- or HO_2^-, and the HO_2^- reaction was reported to be first order in HO_2^- and second order overall.[2] In view of the reactions of O_2 with ruthenium(II) ammines, where O_2^- and H_2O_2 are formed,[3] a mechanism that avoids these species in the reaction with $Fe^{II}(OHP)_3$ would be rather unexpected. The bimolecular rate law for reduction of HO_2^- suggests an outer-sphere electron-transfer mechanism; as pointed out recently by Bakač and Espenson, reports of such a mechanism for reduction of H_2O_2 are extremely rare.[4] In the case of $Cr(CN)_6^{4-}$ the outer-sphere pathway was always a minor term in the rate law,[5] and in the case of $Ru(NH_3)_5L^{2+}$ peculiar saturation effects were observed.[6] The present paper reports substantially different results for the reactions of $Fe^{II}(OHP)_3$ with O_2 and HO_2^-. The substitution reaction of $Fe^{II}(OHP)_3$ with CN^- is also reported.

Experimental Section

Reagents and Solutions. 4,7-Dihydroxy-1,10-phenanthroline (OHP) was purchased from G. F. Smith, and purified by esterification. A 0.5-g sample of the crude ligand was refluxed for 1 h in 10 mL each of acetic anhydride and pyridine. The dark brown suspension was filtered, the filtrate collected, and the solvent removed by rotary evaporation. The

(1) Schilt, A. A. *Analytical Applications of 1,10-Orthophenanthroline and Related Compounds*; Pergamon: New York, 1969.
(2) Ng, F. T. T.; Henry, P. M. *Can. J. Chem.* **1980**, *58*, 1773–1779.
(3) (a) Stanbury, D. M.; Haas, O.; Taube, H. *Inorg. Chem.* **1980**, *19*, 518–524. (b) Stanbury, D. M.; Mulac, W. A.; Sullivan, J. C.; Taube, H. *Inorg. Chem.* **1980**, *19*, 3735–3740. (c) Stanbury, D. M.; Gaswick, D.; Brown, G. M.; Taube, H. *Inorg. Chem.* **1983**, *23*, 1975–1982.
(4) Bakač, A.; Espenson, J. H. *Inorg. Chem.* **1983**, *22*, 779–783.
(5) Davies, G.; Sutin, N.; Watkins, K. O. *J. Am. Chem. Soc.* **1970**, *92*, 1892–1897.
(6) Kristine, F. J.; Johnson, C. R.; O'Donnell, S.; Shephard, R. E. *Inorg. Chem.* **1980**, *19*, 2280–2284.

0020-1669/87/1326-1732$01.50/0